Chapter 8

Accelerated Cavitation Damage of Steels in Liquid Metal Environments

Shengqiang Ma, Jiandong Xing, Hanguang Fu and Shizhong Wei

Additional information is available at the end of the chapter

http://dx.doi.org/10.5772/intechopen.80769

Abstract

Cavitation can be described as a hydrodynamic phenomenon which involves in the formation and collapse of vapor bubbles in a liquid medium. It always accelerates the cavitation damage and brings about multi-scale interactions of cavitation erosion between materials and fluids. For example, corrosion by dissolution/reaction can accelerate cavitation erosion under different liquid temperatures and velocities to alter interface films, and multiphase interface structure can also in turn affect the interfacial flow regime to induce cavitation in various fluids. In this chapter, interfacial characteristics and erosion-corrosion mechanism of directionally solidified (DS) Fe-B alloy with various Fe2B lamellar spacing in flowing zinc were investigated. The results indicate that the formation of adhesive interfacial film not only depends on erosion time and Fe2B lamellar spacing, but also relies on epitaxial ζ accumulation determined by zinc flow effect. Meanwhile, microturbulence of flowing zinc can result in the formation of slip bands and erosion pits on the ζ-FeZn13 surface. The flow-induced localized corrosion appears to accelerate the erosion-corrosion damage of interfacial adhesive film structure and morphology, which reveals underlying erosion mechanism of liquid metal.

Keywords: steel, liquid metal, erosion, adhesive film, flow-induced localized corrosion

1. Introduction

1.1. Foundationals of cavitation

Cavitation is one of the failure and damage in hydraulic machinery and plain bearings. It extensively exists in the contact zone of fluid machinery, pipes, ship propellers, and valves

owing to growth and implosion of cavitation bubbles in flow liquids. Besides, the research on cavitation erosion of materials in liquid metals is very important to ensure the safety and integration of fast breeder reactors using liquid sodium and lead-bismuth eutectic as advanced coolants and to understand cavitation erosion in the liquid mercury target system of the neutron spallation sources. The liquid metal cavitation can be affected by some liquid metal parameters (i.e., its physical properties as well as flow), and it includes liquid properties (i.e., temperature, density of the liquid, sound velocity, etc.) and flow properties (i.e., flow velocity, cavitation number, etc.). Obviously, it differs with other liquidus such as water, solution and liquidus mixtures.

The cavitation process of materials in a flowing liquid corrosive medium first belongs to the mechanical damage. One reason for it is that the cavitation bubbles resulting from dissolved gas or vapor in a flowing liquid at low pressure area can form and grow. Subsequently, the bubble implosion and annihilation can produce shock waves and micro jets, which directly impact on material surface or interface to cause damage. Some investigations indicate that hydraulic parameters can change the cavitation intensity and damage. For example, the cavitation rate generally increases with the improvement of flowing velocity of liquid metal. Other conditions such as temperature and erosion angle of flowing liquid metal also alter the occurrence of cavitation. Recent work also implies that material interface or surface structures can influence the local turbulent/disturbed flow owing to wall/drag effect at these regions. Therefore, the formation of cavitation should be related to the hydromechanics but also linked to the interface construction of materials to synergistically resist cavitation damage, which in turn emphasizes multi-phase and multi-scale interface phenomenon to help us understand the control and design of materials in serious hydraulic mechanical damage. This chapter addresses some aspects of cavitation damage and its control based on the hydraulic parameters and unique interfacial effect.

Liquid metal corrosion differs from the aqueous and acid corrosion (i.e., electrochemical or chemical corrosion with electrolytic ions), which belongs to the physical or physical-chemical process. The liquid metal corrosion mechanism includes several cases: (1) dissolution of solid materials in liquid metal, (2) alloying between liquid and solid metal to form phases, (3) intergranular diffusion penetration, (4) impurity reaction in liquid metal, and (5) thermal and concentration mass transfer. All these processes are involved in environmental factors of medium, metallurgical structure, and stress state of materials, such as temperature fluctuation, surface area to volume ratio, impurity of liquid metal, flow velocity or Reynolds number, erosion angle and intensity, stress intensity, etc.

However, the phenomenon of cavitation on material damage in liquid metal mainly consists of vapor generation and condensation, or the formation of cavitation bubbles/cavities in liquid metal during hydrodynamics, especially for high flowing pressure. This process can cause flowing vibration, increase of hydrodynamic drag or drag flow, changes of flow regime, noise, and the most important of all, cavitation erosion. Rayleigh firstly described the problem of cavitation erosion of ship propellers. After that, numerous investigations on cavitation have been reported to reveal this mechanical damage process. The most important theories on cavitation erosion are microjets and shock waves (or stress waves) during cavitation erosion owing to the implosion/annihilation of bubbles to produce the high intensity damage force on solid materials.

Cavitation erosion mechanism contains two aspects: (1) bubble formation and annihilation involving in the energy transferring into material surface to generate energy superposition; (2) failure mode or cavitation damage mechanism of materials under cavitation. Actually, the cavitation erosion damage is closely related to the surface morphology and roughness of materials, which may affect the amount of bubble nuclei and stagnation pressure of bubbles to increase the occurrence of cavitation crater or fish-scale pits. Therefore, the crater of cavitation erosion often exhibits spongy, honeycomb, and pinhole-shaped and pocking morphologies.

1.2. Background and experimental

Liquid metal corrosion extensively exists in many applications [1, 2]. For example, numerous liquid metals are used for advanced coolant in nuclear equipment, which can cause serious corrosion of nuclear equipment or containers [3–6]. Liquid aluminum can also corrode the casting die in die-casting machine [7]. Another classic case for liquid metal corrosion is the aggressive corrosion and erosion of submerged equipment in hot-dip galvanization [8–10]. The severe corrosion of equipment in liquid zinc results in significant production downtime and huge maintenance costs. Therefore, superior liquid zinc corrosion resistant materials have been constantly designed and developed to meet the requirements of galvanizing equipment [9–11].

Erosion corrosion always witnesses the liquid metal corrosion as a flowing corrosive condition [12, 13]. Wood investigated the synergistic effects of materials under erosion-corrosion environments and implied the mechanical-electrochemical interactions which may influence passive film composition [12, 14]. Besides, Heitz pointed out the chemo-mechanical effect of flow on corrosion from the hydrodynamics and mechanical action of one- and two-phase flows and also emphasized the flow-induced corrosion process [15]. In actual working condition, an interaction or synergistic effect of erosion and corrosion in flowing liquid metal can trigger abnormal premature degradation and destruction of materials to undergo rigorous erosion corrosion [16–18]. Previous investigations revealed the erosion-corrosion interaction of Fe-B alloy in flowing zinc by Al-inhibition addition, and results indicated that pure corrosion and erosion simultaneously affected the total material loss rate [19, 20]. The static corrosion of Fe-B alloy in liquid zinc indicated that a well-adhered interfacial film could gain by controlling the orientation and lamellar spacing of Fe2B to produce a pinning effect at the orientation interface [21, 22]. Moreover, the liquid zinc temperature and Fe2B morphologies (netlike and columnar Fe2B) manifested that the corrosion dominates the product dissolution, while flow erosion governs the Fe2B spalling in flowing liquid zinc, which may depend on the interfacial pinning effect [23, 24]. However, the effect of Fe2B lamellar spacing and product deposition on the film structure and morphology under flowing conditions should emphasize owing to the hydrodynamics of flowing zinc and the effect of flow on corrosion. Besides, there is little research on the interfacial film structure evolution of DS Fe-B alloy with various Fe2B lamellar spacing in flowing liquid zinc. Actually, the phenomena of liquid metal embrittlement and decohesion as well as stress corrosion cracking in flow condition may occur owing to the enhanced chemical and hydromechanical effects (e.g., corrosion-enhanced dislocation emission and effect of flow on corrosion) and segregation-induced reduction of interatomic bond strength [25–29]. Although, many researchers investigated the erosion-corrosion rates

of materials in seawater and aqueous environments with or without solid particles to reveal the synergistic effects [15, 16, 30–32], the relationships between microstructural parameters (e.g., Fe2B lamellar spacing and orientation in flowing zinc) and flow hydrodynamics under erosion-corrosion condition of materials in flowing liquid metal are poorly understood. Dybkov et al. studied the dissolution of a solid in a liquid metal and pointed out that the flowing liquid metal had a strong effect on the thickness of boundary layer and dissolution constant [33–35]. Meanwhile, corrosion interface morphology can directly affect the corrosion process, which may be governed by inhibitors or corrosion barrier [36, 37]. Therefore, erosion corrosion caused by flowing corrosive mediums and material microstructures are of significant importance to probably generate an interface/fluid interaction (e.g., multi-scale material microstructure/environment interactions) on surface films, thus affecting the diffusion, mass transfer, and penetration as well as flow-induced vibration and film rupture during the erosion-corrosion process [27–34, 38, 39].

In present work, the interface film morphology and erosion-corrosion behavior of directionally solidified (DS) Fe-B alloy in flowing zinc have been investigated to reveal the effect of Fe2B lamellar spacing and hydraulic flow on erosion corrosion and interface structures. Accordingly, a flow-induced localized corrosion and cracking is also discussed in flowing liquid zinc based on the Fe2B lamellar spacing regulation, which may understand the combined effects of hydrodynamics and interface film morphology in flowing liquid metal.

1.3. Method and characterization

Erosion sample with dimensions of 140 × 15 × 5 mm^3 was prepared from oriented alloy, dipped into zinc to a depth of 40 mm. Erosion surface of the alloy with Fe2B [001] vertical to the interface was chosen for test owing to the oriented doweling effect. Vertical to interface was chosen for test owing to the oriented doweling effect.

A rotating-disk technique (erosion set-up in **Figure 1a**) was employed to conduct flow zinc erosion test. Erosion thickness loss was obtained by single-side measurement. Then the erosion rate was evaluated using Eq. (1):

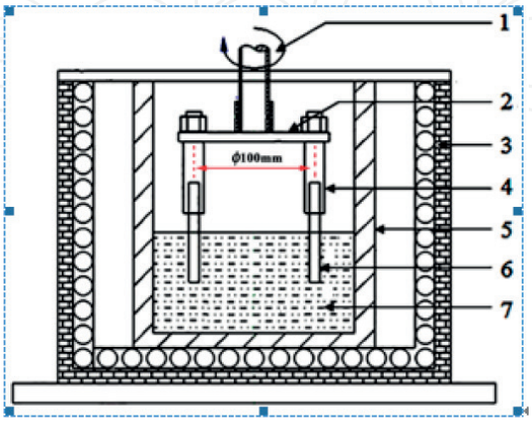

Figure 1. Schematic of erosion testing device: 1-rotating shaft; 2-disk for controlling erosion angle; 3-furance; 4-sample holder; 5-crucible; 6-test sample; and 7-liquid zinc.

$$R = \frac{a-b}{t} \quad (1)$$

where R is the erosion-corrosion rate (μm h^{-1}), a is the original thickness (μm), b is the final thickness (μm), and t is the corrosion time (h).

Microanalysis of the samples was carried out by scanning electron microscopy with back-scattered electron image to identify erosion interfaces. Erosion pit density in layers was performed using Leica Qwin image analysis. The roughness average of layers was measured by colored 3D laser microscope.

2. Results

2.1. As-cast microstructure of DS Fe-B alloy

Figure 2 shows the morphologies and XRD pattern of as-cast DS Fe-B alloy. It can be seen that the longitudinal morphology displays rod-like quadrangular prism along Fe2B [002] orientation (**Figure 2a**). It is a typical dual-phase microstructure with α-Fe and Fe2B. From the transverse section, most of the eutectic Fe2B shows an irregular shape except for some rectangular borides with hollow structures extracted from the DS alloy (**Figure 2b**). **Figure 2c** shows the XRD patterns of the DS Fe-B alloy. Clearly, a strong (002) peak of the Fe2B phase appears in the transverse section, and only a small (004) peak of Fe2B is detected except the (002) plane. However, many crystal planes are detected in the prism. It indicates that [002] orientation of Fe2B is the sole preferred growth direction. In addition, it can be seen that the strongest peak of Fe is the (110) plane, which indicates that α-Fe may grow along [110] orientation under DS condition.

2.2. Effects of erosion time and Fe2B lamellar spacing on erosion-corrosion rate

Figure 3 shows the erosion-corrosion rate of DS Fe-B alloy in flowing zinc as a function of erosion time and Fe2B lamellar spacing (e.g., the spacing between two columnar Fe2B edges showing in **Figure 3a**). It is clear that the erosion-corrosion rate of DS Fe-B alloy with Fe2B [002]

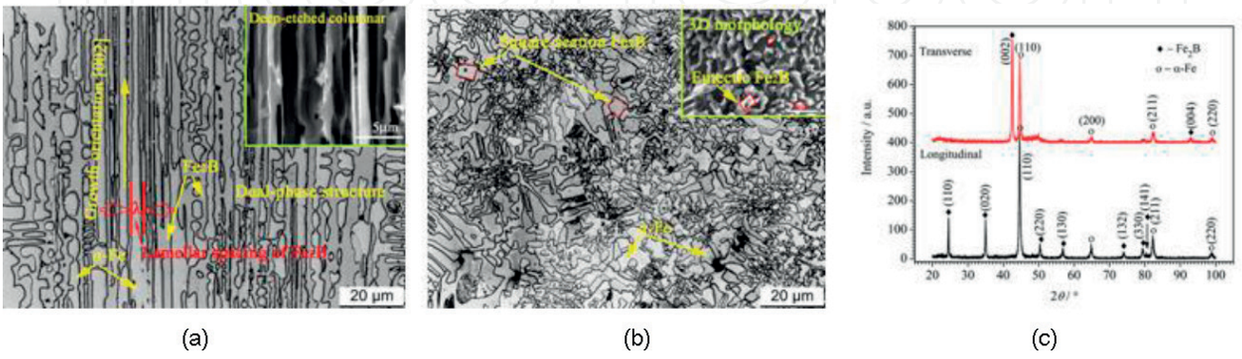

Figure 2. Microstructure and XRD of DS Fe-B alloy: (a) longitudinal; (b) transverse; and (c) XRD.

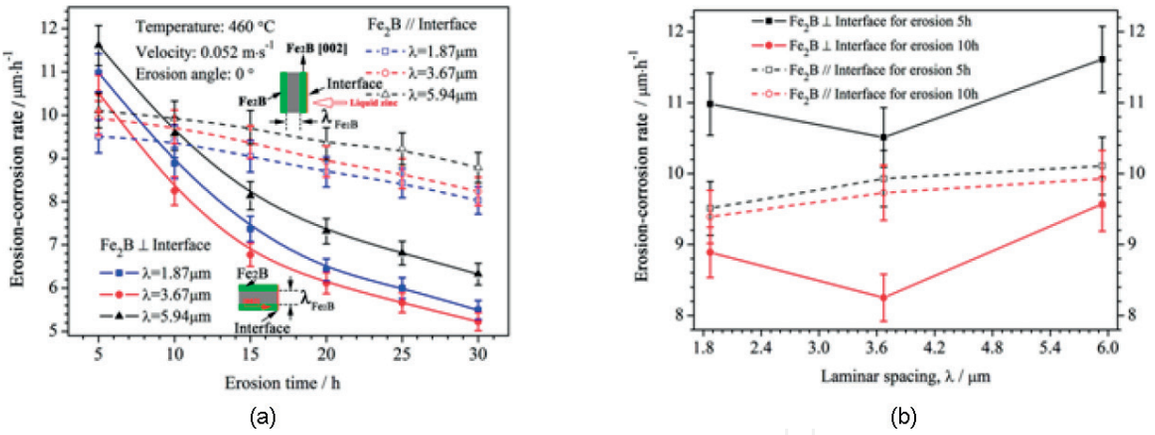

Figure 3. Erosion rates of DS Fe-B alloy with different Fe2B lamellar spacing in flowing zinc: (a) erosion-corrosion rate vs. erosion time; (b) erosion-corrosion rate vs. Fe2B spacing.

orientation perpendicular to the erosion interface decreases sharply at first and then gradually declines to a stable level. However, the erosion-corrosion rate of the parallel sample almost linearly decreases, and it maintains the higher erosion rate after the erosion steps into the steady stage (**Figure 3a**). Compared to two erosion patterns (e.g., vertical or parallel sample), it is revealed that there exists an erosion initiation effect or incubation period of the interface ζ formation for the DS Fe-B alloy in flowing zinc (**Figure 3b**). Obviously, the adhesive film with interfacial pinning effect in the vertical sample at initial erosion-corrosion stage does not form. However, the erosion-corrosion rates decrease with the increase of erosion time, for example, erosion from 5 to10 h (**Figure 3b**).

It indicates that the interface structure may undergo continuous changes owing to the combined effect of the oriented Fe2B and epitaxial grown ζ-FeZn13 products under flow erosion condition. Clearly, epitaxial grown ζ-FeZn13 products at the interface demonstrate an accumulation/pile-up effect and synergistically generate a buffer layer with oriented Fe2B to resist the flowing zinc erosion with the prolonged erosion time. It therefore means that the erosion-corrosion interface structure is dominant by flow-accelerated diffusion of liquid zinc and ζ product accumulation at the interface during the prolonged erosion-corrosion process.

2.3. Interface morphological evolution during flowing zinc erosion corrosion

Figure 4 shows the erosion-corrosion interface of DS Fe-B alloy in flowing zinc with different erosion times as a function of oriented Fe2B lamellar spacing. It is clear that small and large Fe2B spacing in vertical sample in flowing zinc can be damaged in the form of both Fe2B dissolution and numerous spallation at the front of the erosion-corrosion interface for 5 h (**Figure 4a**). Evidently, only suitable lamellar size of oriented Fe2B can resist the erosion corrosion (e.g., λFe2B = 3.67 μm) at the initial erosion stage. However, after erosion for 30 h at a steady erosion stage (**Figure 4b**), there exists an adhesive film with the interfacial pinning effect in DS Fe-B alloy with Fe2B lamellar spacing λFe2B = 3.67 μm. An adhesive product film comprising the oriented Fe2B and epitaxial grown columnar ζ-FeZn13 builds up at the erosion-corrosion interface as a buffer layer to resist flowing liquid zinc damage. Smaller size

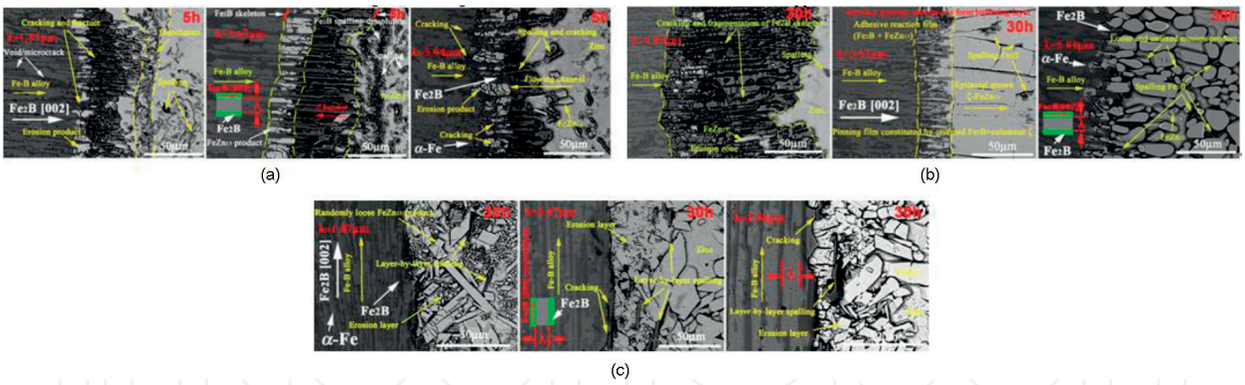

Figure 4. Erosion-corrosion interface morphologies of DS Fe-B alloy with different Fe2B lamellar spacings: (a) vertical sample for erosion 5 h; (b) vertical sample for erosion 30 h; and (c) parallel sample for erosion 30 h.

of Fe2B existing at the erosion-corrosion interface can be seriously destroyed and swept by flowing zinc (**Figure 4b**), while no adhesive film with an interfacial pinning effect develops except for some granular and incompact ζ products when larger size of Fe2B appears (e.g., λFe2B = 5.94 μm) due to their distinctive interface structures and morphologies.

Figure 4c displays the erosion-corrosion interface morphologies of parallel sample erosion for 30 h. Obviously, a layer-by-layer spallation of Fe2B occurs at the erosion-corrosion layer, and there are a plenty of erosion products with different sizes randomly distributed in the layers. The difference of erosion-corrosion interface structure in various Fe2B lamellar spacings is the spalling amounts of Fe2B and products caused by flow, and unsuited Fe2B lamellar spacing can hardly generate adhesive interface and strong synergistic effect of interfacial oriented Fe2B and epitaxial grown ζ-FeZn13 (i.e., multiphase protective film). Therefore, it uncovers that the erosion corrosion strongly refers to not only the interface structure but also the fluid hydrodynamic effects in flowing zinc [14–18, 42].

3. Discussion

3.1. EBSD analysis on microstructure and erosion-corrosion interface

Figure 5 shows the EBSD analysis of DS Fe-B alloy before and after erosion in flowing zinc. Clearly, the DS Fe-B alloy is mainly composed of α-Fe and Fe2B to form dual-phase textured microstructure (**Figure 5a**). The {002} poles of oriented Fe2B grains are located at Y-axis in forms of lightest spot area, while {100}, {110}, and {111} poles of Fe2B grains distribute within quadrants, which indicates that Fe2B [002] orientation dominates its preferred growth direction, as recorded as the strong peak (002) plane in XRD of the transverse section (**Figure 2c**). Furthermore, the {110} poles of α-Fe grains display concentrated spot area in the vertical axis, which may reveal that α-Fe grains generate an orientation growth in the [110] direction.

Figure 5c and **d** show the interfacial orientation map and grain boundary distribution collected by EBSD in a well-distributed directional area of Fe-B alloy in flowing zinc. The

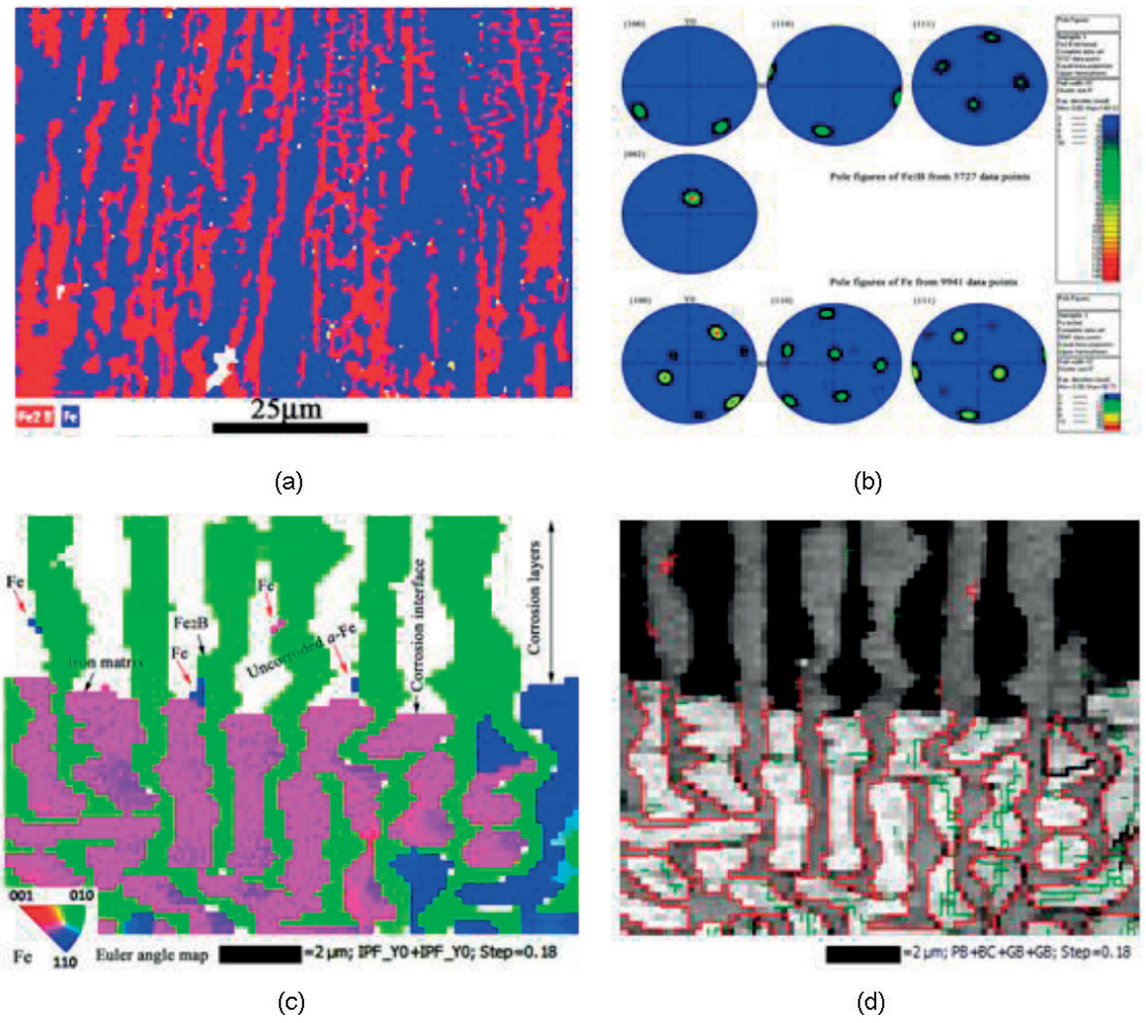

Figure 5. EBSD analysis of DS Fe-B alloy before and after erosion: (a) EBSD image before erosion; (b) pole figures of Fe2B and α-Fe; (c) erosion interfacial Euler angle orientation; (d) grain boundary distribution (black lines indicates misorientations larger than or equal to 10°, green lines indicate grain boundaries with smaller misorientations less than 10°, and red lines indicate phase boundaries).

different colored areas of α-Fe and Fe2B indicate that Fe2B can strongly resist the flowing zinc erosion (**Figure 5c**). However, α-Fe grains in [110] orientation are maintained adjacent to the Fe2B [21], which probably reveals it possesses better corrosion resistance to flowing zinc. Moreover, no selective and preferential erosion-corrosion path occurs on α-Fe/Fe2B phase boundary, and α-Fe still displays uniform dissolution in flowing zinc (**Figure 5d**). That means the phase boundary in DS Fe-B alloy does not demonstrate obvious corrosion sensitivity in liquid zinc. Obviously, the erosion corrosion of DS Fe-B alloy in flowing zinc largely relies on the adhesive interface structure controlled by Fe2B lamellar spacing and dense pile-up effect of epitaxial grown ζ-FeZn13 at the interface.

Nevertheless, such an interface structure can be forcefully affected by the flow pattern, which is based on the dimensionless parameters, for example, Reynolds number (Re), Sherwood number (Sh), and Schmidt number (Sc) [13, 15]. According to the Refs. [6, 15, 41–43], the fluid flow under rotating condition should be turbulent flow if the Reynolds number Re is more

than 200. In the present rotating disk, the bulk flowing pattern should be regarded as turbulent flow owing to the estimated Re value (here Re = 8066). Therefore, there should be a violent and sustaining fluid force of flowing zinc, which can strongly impinge on the erosion interface to break the Fe2B skeleton (**Figure 4**). The damaged erosion interface indicates that hydraulic effects from fluid scouring force and momentum transfer may strongly destroy the surface film and sweep ζ products, thus accelerating the further localized corrosion [15, 41–44].

3.2. Erosion-corrosion synergistic effects on interfacial morphologies

Figure 6 shows the occurrence of cracks along the α-Fe/Fe2B boundary and transgranular cracking of Fe2B. Obviously, no corrosion products generate along the α-Fe/Fe2B phase boundary, and only initiation and propagation of cracking occurs ahead of the erosion-corrosion interface in some weak sites [25–28, 42–46]. The separation of α-Fe/Fe2B phase boundary indicates that high zinc potential and penetration under capillary action can induce the weakening of phase boundary [13, 21, 25–28, 40]. Actually, the high zinc potential at the interface may induce the reduction of the cohesion strength along the weak site of the phase boundary [21, 40]. Essentially, a highly concentrated stress zone ahead of the erosion-corrosion interface can produce because of the growth of products. Thus, the combined effect from scouring force of flowing zinc and high zinc potential can stimulate this stressed zone to initiate cracks without products at the interface owing to the chemical and mechanical effect (**Figure 6a**) [15, 21, 25–29, 40, 42].

From **Figure 6b**, it reveals that the Fe2B (i.e., nonwetting with liquid zinc) is directly prone to cracking through transgranular pattern with a main crack plus some network of microcracks to release the high zinc potential energy. Obviously, the location of cracking initiation occurs in the reduced bonding site at the front of the erosion interface, and there is almost no products existing on the cracking interface (**Figure 6b**). Therefore, once the cracks take place under the hydrodynamic effect and high potential of flowing liquid zinc, the strong capillarity and

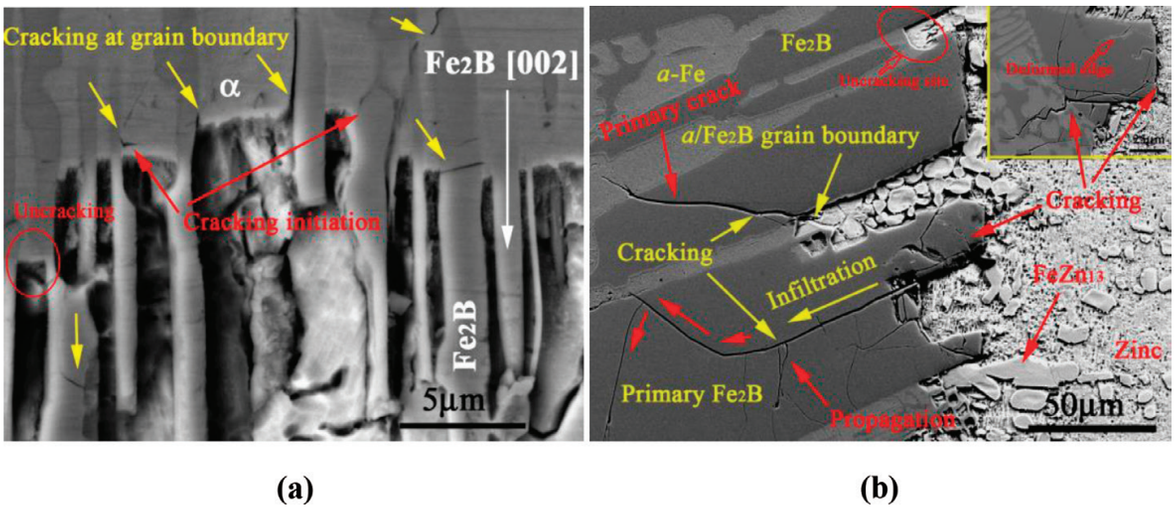

Figure 6. Cracking along α-Fe/Fe2B boundary and transgranular cracking of Fe2B in flowing zinc: (a) phase boundary cracking; (b) transgranular cracking of Fe2B.

penetration of liquid zinc along these defects as attacking channel occur, thus leading to large cracking spreading and spalling of Fe2B as well as film breakdown of layers [14–17, 41–46].

Figure 7 shows the changes of the interface and layers of DS Fe-B alloy under the flowing zinc erosion corrosion. It is clear that the plenty of columnar Fe2B produces cracking and fracture at the erosion interface, which results from the local stress concentrations produced by high zinc potential, fluid force effect, and a small quantity of growth stress of products. The localized corrosion accelerated by the flowing erosion and corrosion cracking should be responsible for the overall damage of the interfacial films [43–46]. The slip bands of products and cracks of Fe2B in the layers reveal the powerful combined effects of chemical and mechanical damage on the films (**Figure 7a**). In nature, local corrosion and flow regime may fully induce and stimulate to emit the dislocation motion and crack initiation in such viscous flowing media [26–29, 45, 46]. **Figure 7b** and **c** show the corrosion of matrix at the front of the erosion-corrosion interface. Evidently, some spalling debris of matrix separated from the substrate can scatter among the corrosion products (**Figure 7b**). Meanwhile, the interfacial front of the erosion reveals a thin loose and porous structure of ferritic layer (**Figure 7c**), which can collapse into small broken pieces and debris before its corrosion owing to the flow effect. Essentially, a deformed sublayer with higher stress concentration at the erosion-corrosion interface may generate under local turbulent flow, which makes the sublayer of ferrite matrix porous to facilitate the further corrosion [41, 42]. Besides, the flowing role can enhance the penetration of liquid zinc into the substrate. **Figure 7d** shows a classic penetration of liquid zinc through the grain boundary. It reveals that the flowing zinc runs through several

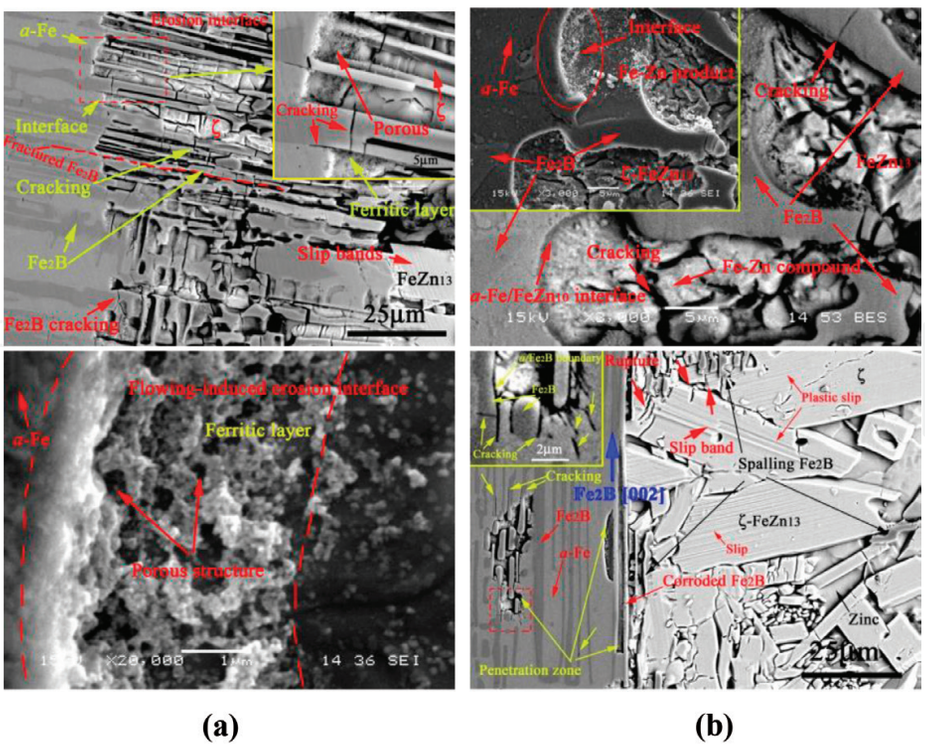

Figure 7. Interface changes of DS Fe-B alloy (λFe2B = 3.67 μm): (a) microcracks; (b) and (c) matrix zone with porous structures; and (d) penetration, surrounding cracking, and slip bands of ζ products.

grains and penetrates into the inner grains far away from the erosion-corrosion interface. Surrounding these penetration areas, a small amount of corrosion product generates, and more cracking initiation and propagation occur at the edge of the corrosion areas (**Figure 7d**). It is revealed that the cracking produces at the phase boundary without any products, which further indicates that a film stress and decohesion at phase boundary occur since the segregation energy under high zinc potential [45, 46]. In addition, numerous plastic slip bands and spalling of Fe2B happen on the surface of the products (ζ-FeZn13), and larger cracks appear ahead of the Fe2B rupture fronts, which is attributed to the stress concentration in the flowing circumstance owing to the shear force of local liquid zinc turbulence [41–44].

3.3. Flow-induced corrosion cracking and pits in erosion-corrosion layers

Figure 8 shows the flowing zinc scouring effect on the damage of the erosion-corrosion layers. It is clear that the flowing zinc can scour and sweep the interface adhesive film, peeling off the interface (**Figure 8a**). The overall fracture and rupture of eroded Fe2B skeleton indicate that the flow force of liquid zinc can pull apart and drag films from the interface. Besides, typical erosion-corrosion pits and plastic slips as well as plenty of cracking spalling Fe2B around the erosion interface can coexist. That is to say, an interface adhesive film withstands severe liquid zinc erosion corrosion, which also aggravates a phase transition layer of Fe2B skeleton (**Figure 8a**) [21, 40]. Obviously, three zones, that is, I-zone with uncorroded Fe2B, II-zone with the corroded Fe2B (namely, transition phase in dark gray color in **Figure 8a** and **b**), and III-zone with columnar ζ-FeZn13 products [40], are included. Obviously, a strong combined effect between erosion and corrosion by flowing zinc concurrently happens to damage the interface film. The repaired film behind the spalling blocks (**Figure 8b**) implies that a synergistic role of flow and corrosion can accelerate the zinc diffusion reaction and product accumulation to rebuild the broken films. Actually, strong local turbulent flow can assist the occurrence of corrosion, thus leading to the flow-induced localized corrosion (FILC) [38, 39, 41–46]. From **Figure 8c**, it is clear that numerous teardrop- and horseshoe-shaped continuous erosion pits (i.e., micromechanical pits by flow) intensively appear on the surface of ζ products. Obviously, each erosion pit has a sharp inverted triangle at the bottom of the sunken pits, and they can arrange linearly and regularly along the plastic slip line. Besides, some big pits emerge accompanying with some slips in it from the combination of small pits. The aggregation cracking

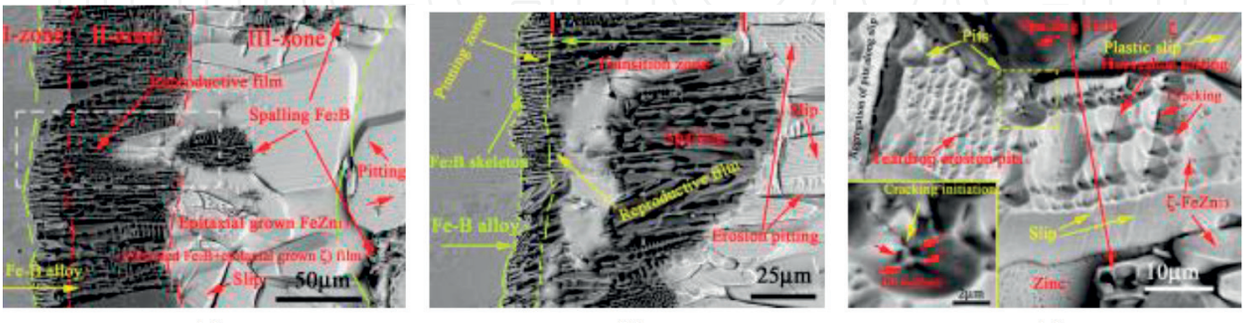

Figure 8. Effects of flowing zinc scouring on the damage of erosion layers: (a) and (b) rupture and phase transition of Fe2B; (c) pits and cracking along the slip as well as the aggregation of small erosion pits.

of small erosion pits along slip indicates that large stress concentration occurs along the slip direction [28, 45]. Meanwhile, a small tiny crevice surrounded by some cracks generates at the bottom of the larger erosion pits, which actually reveals that each pit may incubate and initiate microcracks at the bottom of the erosion pits related to the flow-induced stress cracking along slip bands. Evidently, the erosion damage is much larger than that of corrosion, and flow-assisted localized corrosion can enhance. Besides, the dislocation motion may emit to induce some deformations, and cracks initiate in the layers, which is responsible for the stress concentration based on the flow force and film stress [45, 46]. Therefore, a fierce synergistic effect of erosion and corrosion in flowing zinc occurs at the erosion interface.

3.4. Effect of Fe_2B lamellar spacing on the interface structure in flowing zinc

Figure 9 shows the bending deformation and corrosion pitting (i.e., chemical pits from pitting corrosion) of Fe2B in DS Fe-B alloy with different lamellar size in flowing zinc. From **Figure 9a**, it reveals the micromechanical effect on the bending deformation and fracture of smaller borides at the front of the erosion interface. Clearly, a lot of bending deformation of borides occurs at the Fe2B/ζ erosion interface, and little corrosion products generate among the oriented Fe2B (e.g., λFe2B = 1.87 μm). Instead, numerous small gaps among Fe2B facilitate the occurrence of the liquid zinc flowing scouring effect in columnar grains. The cracking and bending deformation at the erosion interface along the flow direction can fully indicate that attacking shear force strongly impinges on the interface to destroy the corrosion-resistant phase and film microstructure (**Figure 9a**). Actually, the large turbulent flow (e.g., occurrence of fluid whirlpool when encountering obstacles) can induce the cracking initiation of Fe2B and result in its rupture. However, no obvious deformation of borides with moderate lamellar spacing (i.e., λFe2B = 3.67μm) takes place, and only numerous pitting corrosions (e.g., smallpox petechial or freckles of pitting corrosion) triggers on the Fe2B surface (**Figure 9b**). It also infers that large absorption under high potential leads to decohesion firstly, and then chemical reaction occurs between free atoms or ions to produce Fe2B pitting corrosion stimulated by flow (e.g., free iron and boron atoms releasing from Fe2B lattice to complete Fe2B/FeB phase transition through atomic configuration) [14, 40]. The visible cracking and pitting of borides at the erosion interface indicate that the erosion damage not only depends on local

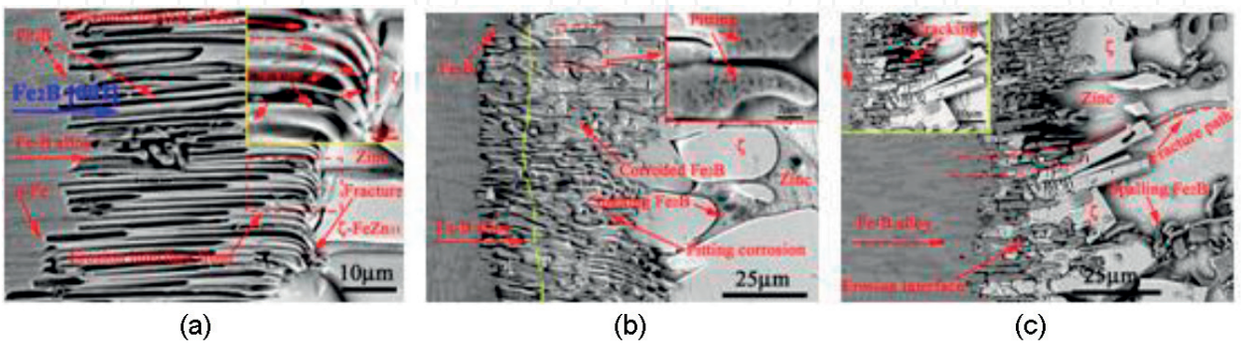

Figure 9. Bending deformation and pitting corrosion of Fe2B in DS Fe-B alloy with different lamellar sizes in flowing zinc: (a) deformation of Fe2B at erosion interface front (λFe2B = 1.87 μm); (b) pitting corrosion of Fe2B (λFe2B = 3.67 μm); and (c) cracking and fracture of Fe2B in layers (λFe2B = 5.94 μm).

turbulent intensity, but also relies on thickness of boride (i.e., lamellar spacing) to sustain flow scouring. Therefore, the local turbulence and induced pitting corrosion can strongly determine the damage of the interface films and mass transfer owing to the size effect of Fe2B lamellae.

Figure 10 shows the EBSD erosion-corrosion morphology and the corresponding electron black-scattered pattern (EBSP) in interface layers. It is clear that the boride lateral displays an obvious cavernous sculpture or fish-scale shaped craters, which reveals that the erosion corrosion of Fe2B occurs gradually (**Figure 10a**). At the Fe2B/FeZn13 interface, numerous erosion pits and some slip steps as well as cracks ahead of the slips indicate that the laterals of Fe2B (e.g., (110) prism) are prone to more eroded than that of the basal plane (e.g., (001) plane), which may be related to the zinc-atom penetration potential and corroded anisotropy of Fe2B (**Figure 10b**) [40].

3.5. Erosion-corrosion mechanism determined by interface structure and flow

Theoretically, the breakdown and subsequent repair of the protective films depend on the localized turbulence at the erosion-corrosion interface. That means flow-induced localized corrosion (FILC) may emerge in turbulent zone during the erosion process [43–46]. Essentially, there exist velocity and concentration boundary layers determined by the rate-controlled step during the erosion-corrosion process [41, 42, 47–49].

Figure 11 depicts a schematic representation of interface damage and flow-accelerated corrosion (FAC) of the DS alloy in flowing zinc with the increase of fluid velocity or shear intensity. It is revealed that when an adhesive interfacial pinning film (i.e., oriented Fe2B plus epitaxial grown ζ-FeZn13) exists at the erosion-corrosion interface, a tiny fluctuation of fluid velocity may result in the occurrence of microturbulence among the orientation grains or gaps of product films. Once the liquid zinc velocity reaches the threshold level, the interface film will destroy, and then the thinning and breakaway of the films may occur [6, 29]. Actually, local microturbulence is likely to generate in the form of fluid eddies or reversed flow owing to the presence of the obstacles. That means a steady erosion-corrosion stage will be suppressed (i.e., stage-I in **Figure 11**). In this situation, the film will be constantly thin and attenuate fast, thus leading to the increase of the erosion-corrosion rate. Besides, the penetration of

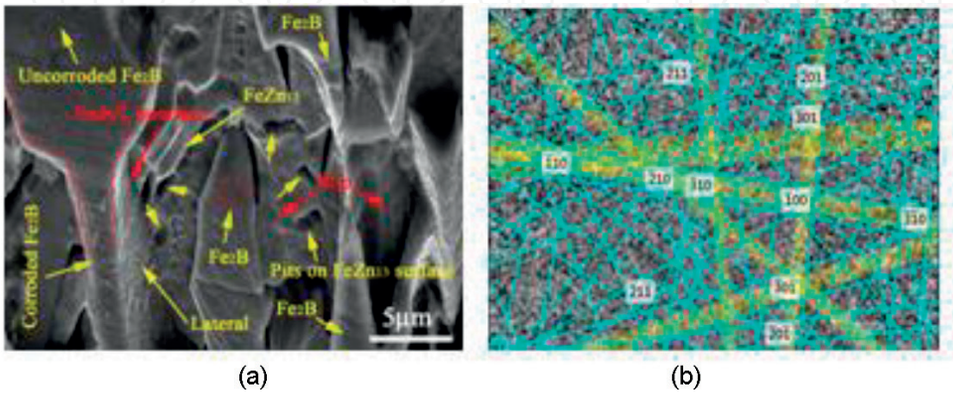

Figure 10. EBSD erosion-corrosion morphology and electron black-scattered pattern (EBSP) of Fe2B in erosion layers: (a) morphology at the interface; (b) EBSP of Fe2B.

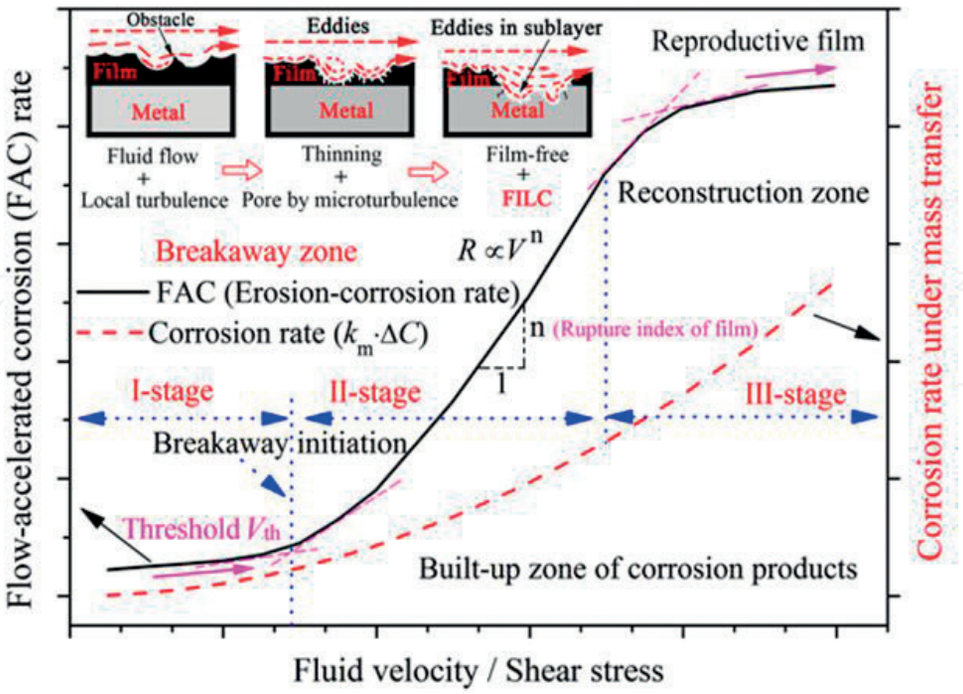

Figure 11. Schematic erosion-corrosion mechanism and interface damage under flow-accelerated corrosion (FAC) of the DS alloy in flowing zinc.

liquid zinc in boundaries and stressed zones ahead of the products may strongly induce interatomic decohesion and segregation [14, 26–28]. The flow-induced localized corrosion on the bare and uncovered matrix as well as some microcracks generating at weak cohesion can burst out, which in turn roughens the interface (e.g., the stage-II in **Figure 11**) [6, 15, 29, 41–44]. Meanwhile, the corrosion products are swept away endlessly by strong flowing zinc in order to reject their deposition and accumulation at the interface. Therefore, a strong synergistic effect of microturbulence and FILC can generate, which depends on the interface film structure and morphology. Accordingly, the present work reveals the importance of interface morphology and effect of Fe2B size on interfacial film damage.

4. Conclusions

This work reveals the interface structure and film damage of DS Fe-B alloy with various Fe2B lamellar spacing in flowing zinc as well as the relationship between the interfacial morphology and local flow. The main conclusions are as follows:

1. The directional Fe-B alloy with Fe2B [002] orientation perpendicular to the erosion-corrosion interface possesses the best erosion-corrosion resistance to flowing zinc when Fe2B lamellar spacing equals to 3.67 μm in present conditions.
2. Interfacial Fe2B undergoes strong flowing zinc erosion and cracking at initial erosion-corrosion stage to form a dissolution layer. Besides, the α-Fe/Fe2B phase boundary in DS Fe-B alloy cannot demonstrate obvious corrosion sensitivity.

3. Local turbulence of liquid zinc can cause the formation of slip bands and erosion-corrosion pits on the surface of ζ-FeZn13, subsequently leading to the aggregation and crack initiation of erosion pits along slips.

4. The erosion-corrosion mechanism dominates the combined effects of breakdown of films, the rupture of Fe2B, and flow-accelerated corrosion, which depends on the Fe2B lamellar spacing controlled interface structures and morphology.

Acknowledgements

The authors thank the financial support for this work from the Natural Science Foundation of China (No. 51771143, 51301128 & 51475005), and also appreciate the Open Fund of National Joint Engineering Research Center for abrasion control and molding of metal materials (Grant No. HKDNM201801) for this work.

Conflict of interest

The entirety of this text with the 'conflict of interest' declaration is indicated.

Author details

Shengqiang Ma[1]*, Jiandong Xing[1], Hanguang Fu[2] and Shizhong Wei[3]

*Address all correspondence to: sqma@mail.xjtu.edu.cn and shengqiang012@163.com

1 State Key Laboratory for Mechanical Behavior of Materials, School of Materials Science and Engineering, Xi'an Jiaotong University, Xi'an, Shaanxi Province, P.R. China

2 Research Institute of Advanced Materials Processing Technology, School of Materials Science and Engineering, Beijing University of Technology, Beijing, P.R. China

3 National Joint Engineering Research Center for Abrasion Control and Molding of Metal Materials, Henan University of Science and Technology, Luoyang, P.R. China

References

[1] Fernandes PJL, Jones DRH. International Materials Reviews. 1997;**42**:251-261

[2] Ina K, Koizumi H. Materials Science and Engineering A. 2004;**387-389**:390-394

[3] Zhang J, Hosemann P, Maloy S. Journal of Nuclear Materials. 2010;**404**:82-96

[4] Suzuki T, Ohno K, Masuda S, Nakanishi Y, Matsui Y. Journal of Nuclear Materials. 1987;**148**:230-234

[5] Antill JE, Peakall KA, Smart EF. Journal of Nuclear Materials. 1975;**56**:47-60

[6] Balbaud-Célérier F, Barbier F. Journal of Nuclear Materials. 2004;**289**:204-209

[7] Tang N, Li YP, Koizumi Y, Kurosu S, Chiba A. Corrosion Science. 2013;**75**:262-268

[8] Ma SQ, Xing JD, Fu HG, Yi DW, Zhang JJ, Li YF, et al. Corrosion Science. 2011;**53**:2826-2834

[9] Wang WJ, Lin JP, Wang YL, Chen GL. Corrosion Science. 2007;**49**:1340-1349

[10] Liu XB, Barbero E, Xu J, Burris M, Chang KM, Sikka V. Metallurgical and Materials Transactions A: Physical Metallurgy and Materials Science. 2005;**36**:2049-2058

[11] Liu Y, Tang MY, Song YY, Wu CJ, Peng XP, Su XP, et al. Surface and Coating Technology. 2015;**276**:714-720

[12] Richardson T. Chapter 2.13 flow-assisted corrosion. In: Schmitt HG, Bakalli M, editors. Shreir's Corrosion. 1st ed. A division of Reed Educational and Professional Publishing Ltd; 2010;**1**:954-1004. ISBN 0 7506 1077 8

[13] Liu GZ, Ma SQ, Xing JD, Fu HG, Gao Y, Bai YP, et al. Journal of Materials Research. 2015;**30**:727-735

[14] Wood RJK. Wear. 2006;**261**:1012-1023

[15] Heitz E. Electrochimica Acta. 1996;**41**:503-509

[16] Jiang J, Stack MM, Nevile A. Tribology International. 2002;**35**:669-679

[17] Wood RJK, Wharton JA, Speyer AJ, Tan KS. Tribology International. 2002;**35**:631-641

[18] Wharton JA, Wood RJK. Wear. 2004;**256**:525-536

[19] Wang Y, Xing J, Ma S, Liu G, Jia S. Materials Science and Technology. 2016;**32**:49-56

[20] Wang Y, Xing JD, Ma SQ, Zheng BC, Fu HG, Liu GZ. Corrosion Science. 2016;**112**:25-35

[21] Ma SQ, Xing JD, He YL, Fu HG, Li YF, Liu GZ. Acta Materialia. 2016;**115**:392-402

[22] Wang Y, Xing JD, Ma SQ, Zheng BC, Liu GZ, Yang DX, et al. Corrosion Science. 2016;**104**:260-268

[23] Wang Y, Xing JD, Ma SQ, Liu GZ, He YL, Yang DX, et al. Corrosion Science. 2015;**98**:240-248

[24] Wang Y, Xing JD, Ma SQ, Liu GZ, Fu HG, Jia S. Journal of Materials Engineering and Performance. 2015;**24**:2444-2450

[25] Gibson MA, Schuh CA. Acta Materialia. 2015;**95**:145-155

[26] Gutman EM. Surface and Coating Technology. 1994;**67**:133-136

[27] Zhu LK, Yan Y, Li JX, Qiao LJ, Li ZC, Volinsky AA. Corrosion Science. 2015;**100**:619-626

[28] Revie RW. Progress in Surface Science. 1983;**14**:53-112

[29] Li JX, Chu WY, Wang YB, Qiao LJ. Corrosion Science. 2003;**45**:1355-1365

[30] Burstein GT, Sasaki K. Wear. 2000;**240**:80-94

[31] Malka R, Nešić S, Gulino DA. Wear. 2007;**262**:791-799

[32] Uchida S, Naitoh M, Okada H, Uehara Y, Koshizuka S. Nuclear Engineering and Design. 2011;**241**:4585-4593

[33] Barmak K, Dybkov VI. Journal of Materials Science. 2003;**38**:3249-3255

[34] Barmak K, Dybkov VI. Journal of Materials Science. 2004;**39**:4219-4230

[35] Kassner TF. Journal of the Electrochemical Society. 1967;**114**:689-694

[36] Robbiola L, Blengino JM, Fiaud C. Corrosion Science. 1998;**40**:2083-2111

[37] Zhang JS. Corrosion Science. 2009;**51**:1207-1227

[38] Blevins RD. Progress in Nuclear Energy. 1979;**4**:25-49

[39] Hurricks PL. Wear. 1970;**15**:389-409

[40] Ma SQ, Xing JD, Fu HG, He YL, Bai Y, Li YF, et al. Corrosion Science. 2014;**78**:71-78

[41] Poulson B. Corrosion Science. 1983;**23**:391-430

[42] Heitz E. Corrosion. 1991;**47**:135-145

[43] Silverman DC. Corrosion. 1984;**40**:220-226

[44] Schmitt G. Materials and Corrosion. 2001;**52**:329-343

[45] Gao KW, Chu WY, Gu B, Zhang TC, Qiao LJ. Corrosion. 2000;**56**:515-522

[46] Wang WW, Zhang ZL, Ren XC, Guan YJ, Su YJ. Scientific Reports. 2015;**5**:10579-10689

[47] Giorgi ML, Durighello P, Nicolle R, Guillot JB. Journal of Materials Science. 2004;**39**: 5803-5808

[48] Dybkov VI. Reaction Diffusion and Solid State Chemical Kinetics. 1st ed. Kyiv, Ukraine: IPMS Publications; 2013

[49] Cussler EL. Diffusion Mass Transfer in Fluid System. 3rd ed. UK: Cambridge University Press; 2007

IntechOpen